

Monolayer Plasma Crystals: Experiments and Simulations

J. Goree, D. Samsonov, Z. W. Ma, A. Bhattacharjee
Dept. of Physics and Astronomy, The University of Iowa, Iowa City, Iowa 52246

H. M. Thomas, U. Konopka, G. E. Morfill
Max-Planck Institute for Extraterrestrial Physics, 85740 Garching, Germany

Abstract. Experiments and simulations are reported for two kinds of monolayer plasma crystals. In a monolayer with a small number of particles, ranging from 1-19, we measured the microscopic structure of very small crystals. The crystals have concentric rings. For certain numbers of particles, corresponding to 'closed-shells' in the outermost ring, the configurations are the same as for hard spheres. Yukawa molecular-dynamics simulations accurately reproduce our experimental results. By adding far more particles (~10,000) and operating at higher power, we discovered Mach cones. These are V-shaped shocks created by supersonic objects. They were detected in a two-dimensional Coulomb crystal. Most particles were arranged in a monolayer, with a hexagonal lattice in a horizontal plane. Beneath the lattice plane, a sphere moved faster than the lattice sound speed. The resulting Mach cones were double, first compressional then rarefactive, due to the strongly-coupled crystalline state. Molecular dynamics simulations using a Yukawa potential also show multiple Mach cones.

INTRODUCTION

Many experimenters have reported Coulomb crystals in dusty plasmas (1-13). In this paper, we report experiments and simulations with monolayer Coulomb crystals. These were carried out by suspending microspheres in a horizontal electrode sheath. Two experiments were performed.

In the first experiment, we prepared crystals with small numbers of particles, ranging from 1-19 particles. These configurations are arranged in concentric shells. These arrangements can be categorized, as a function of particle number, as a "periodic table" of small plasma crystals.

In the second experiment, which was carried out with ~10,000 microspheres in the monolayer, we observed Mach cones. These are V-shaped shock waves produced by supersonic particles. Mach cones are familiar in the field of gasdynamics (14) where they are created, for example, by supersonic aircraft. Less commonly, Mach cones also occur in solid-state matter. For example, surface waves along a borehole, in seismographic testing, propagate faster than the sound speed in solid rock, thereby creating Mach cones in the rock (15).

The existence of Mach cones in dusty plasmas was predicted theoretically by Havnes *et al.* (16). Moreover, they predicted that Mach cones are produced in the dust

of Saturn’s rings by boulders moving in Keplerian orbits. Dust moves at a different speed, nearly co-rotational with the planet. In the case of Saturn’s rings, the dust is probably weakly-coupled, and the relevant sound wave would be the Dust Acoustic Wave (DAW).

PERIODIC TABLE EXPERIMENT

In the experiment, we used a modified GEC reference cell with a capacitively-coupled lower electrode. By filling the chamber to a low pressure of 55 mTorr, and applying a 166 V peak-to-peak radio-frequency voltage at 13.56 MHz, we produced a Krypton glow discharge. The dc self bias was -55 V, and the Debye length measured by a Langmuir probe and using the ABR method, is estimated as 370 μm .

We used microspheres of diameter 8.9 ± 0.1 μm and density 1.51 g/cm^3 . By dropping these through a 1-mm opening in an upper electrode, we were able to introduce only one sphere at a time. After it came to equilibrium, we imaged it, using a 512×512 resolution digital camera equipped with a Nikon micro lens. Then we added a second particle, and so on.

The particle charge was measured as $Q = -12,300 e$, using a variation of the resonance method of Melzer and Trottenberg (4,5). Our variation avoids Langmuir-probe measurements of ion density, which can have uncertainties of a factor of 3 or more due to various factors including placing the probe at a location other than the particle height. Instead, we use measurement of the dc self bias, dc plasma potential, and particle levitation height, which can be measured more accurately. Using the assumptions that the dc electric potential in the sheath varies quadratically with height and that the particle height is determined by a force balance with gravity but not ion drag, we are able to compute the particle charge with a small random error.

Particle x - y coordinates were identified from the camera images, and then plotted, as in Fig. 1. We applied Delaunay triangulation to show the bond configuration.

For comparison, we also show results from a Yukawa molecular dynamics simulation, which is described later. The simulation parameters were $Q = -15,300 e$, $\lambda_D = 370$ μm , $m = 5.57 \times 10^{-10}$ g, and the curvature of the confining potential was parameterized by $k = 1.15 \times 10^{-8}$ g/s^2 .

We also show results for a hard-sphere experiment, which was carried out simply by dropping metal balls into a spherical bowl.

We found that plasma crystals at the smallest size are predictable. Their positions are accurately modeled by a Yukawa simulation. We believe that the Yukawa potential is suitable because the particles lie in a two-dimensional plane that is perpendicular to the ion flow. In a three-dimensional crystal, it is known that ion focusing leads to strongly non-isotropic potentials that cannot be modeled accurately with a Yukawa potential (17).

Certain numbers of particles have multiple multiple stable equilibria. One might call these “isotopes.” These were most easily identified in the numerical simulations, which we repeated for 100 different random initial seedings of particle positions.

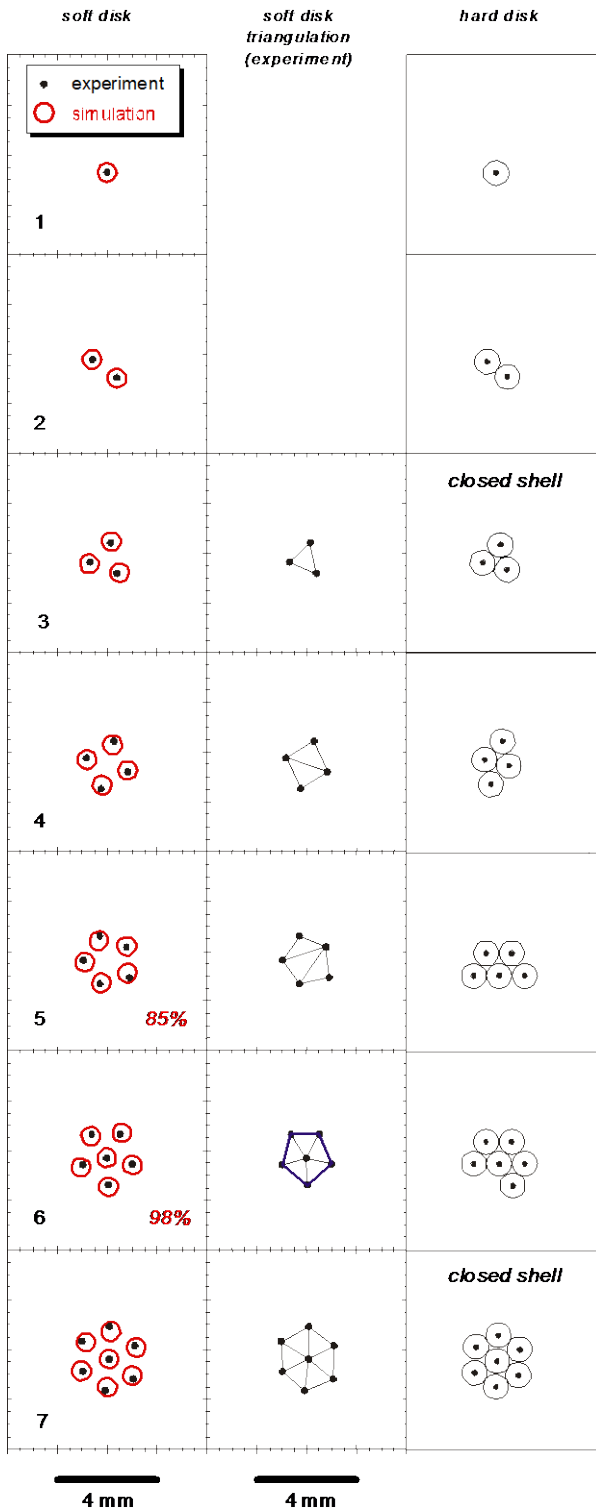


FIGURE 1. Particle configurations from the dusty plasma experiment are shown with dots in the left column, and in the Delaunay triangulation in the center column. (continued next page)

FIGURE 1. (continued) Simulation results are shown as open circles in the left column. In some panels, a percentage is indicated, showing the fraction of simulation runs that yielded the equilibrium (isotope) shown; other runs resulted in different isotopes. Hard disk experiment results are shown in the right column. These results are the beginning of a series for particles 1-19. The complete results will be presented elsewhere.

Comparing the dusty plasma results to the hard-sphere analog, we find that the plasma crystal tends to arrange with an azimuthally-symmetric outer ring, whereas the hard spheres arrange in a perfect triangular pattern even if the outer ring is incomplete. For certain numbers corresponding to complete shells, the two are the same. This occurred for 3, 7, 12, and 19 particles.

Further details of these experiments and simulations will be reported elsewhere.

SIMULATION

We performed molecular-dynamics simulations of the experiments. Particles were constrained to move in a horizontal plane. The particle equation of motion $m d^2 \mathbf{r} / d t^2 = - Q \nabla \varphi - \gamma d \mathbf{r} / d t$ was integrated for N particles. The electric potential φ consisted of a parabolic potential to model the radial confinement from the plasma, plus a Yukawa inter-particle repulsion, $\varphi = - k r^2 / 2 - \sum (Q / r_i) \exp (-r_i / \lambda_D)$. Here r is the distance from the central axis, r_i is the distance to particle i , and the sum is over all other particles. The parameter k determines the curvature of the bowl-shaped confining potential. The particles were loaded with random initial positions, and then their motion was followed by integrating their equations of motion simultaneously, using a simple leapfrog integrator. Their motion eventually ceased, as the excess kinetic energy was dissipated by drag, $\gamma d \mathbf{r} / d t$, leaving the particles in a stable equilibrium.

MACH CONE EXPERIMENT

Our experiments were carried out in a strongly-coupled plasma, with a particle separation that was smaller than the Debye length. Under these conditions, the sound wave is the Dust Lattice Wave (DLW), which is different from the DAW that propagates under other conditions. The results we report here are peculiar to the crystalline strongly-coupled state. We expect that certain Mach cone features, which we will identify, will be different in a weakly-coupled dusty plasma.

We used a larger 230 mm diameter electrode, without a glass insert in the upper ring electrode. Krypton gas was used at the low pressure of 0.05 mBar. Higher pressures result in a damping rate too high to observe mach cones. Approximately 10^4 microspheres were shaken into the plasma above the electrode. The rf input power was much higher than in the periodic table experiment. We operated at 50 W, yielding

a self-bias of -245 V on the lower electrode. This bias levitated the negatively-charged particles 6.5 mm above the lower electrode. In the radial direction a gentle ambipolar electric field trapped the particles in a disk approximately 40 mm in diameter. This disk, which we term the “lattice layer,” was a two-dimensional lattice, with a particle spacing $\Delta = 256 \mu\text{m}$. The Debye length was smaller, $\lambda_D = 124 \mu\text{m}$, with an accuracy of a factor of two. There was very little particle motion.

Mach cones in the lattice layer were produced by charged particles moving in a second incomplete layer, 200 μm beneath the lattice layer. This lower layer was populated by less than 10 particles. Unlike the particles in the lattice layer, they moved rapidly in the horizontal direction. Presumably they were accelerated by a horizontal electric field in the sheath, which we cannot explain. Sometimes they traversed the entire disk in a nearly straight line. They may have been single spheres or agglomerates of two or three.

Imaging the cones with the digital camera and a horizontal laser sheet, we observed the Mach cones in the lattice layer. These cones are easily seen in the moving video, but more difficult to identify in a still image. The video rate was 50 frames/sec.

To process the data to produce a still image of a Mach cone, we carried out the following computational process. Images were analyzed to identify the x-y coordinates of the particles. Particles were threaded from one image to the next, and their velocity was computed as the change in position, divided by the 0.02 sec frame interval. Then, by computing the magnitude of the velocity vector, we produced a map of the particle speed. To reduce noise, we averaged this over nine consecutive frames, which we displaced spatially so that the position of the fast particle coincided. This yielded the image shown in Fig. 2.

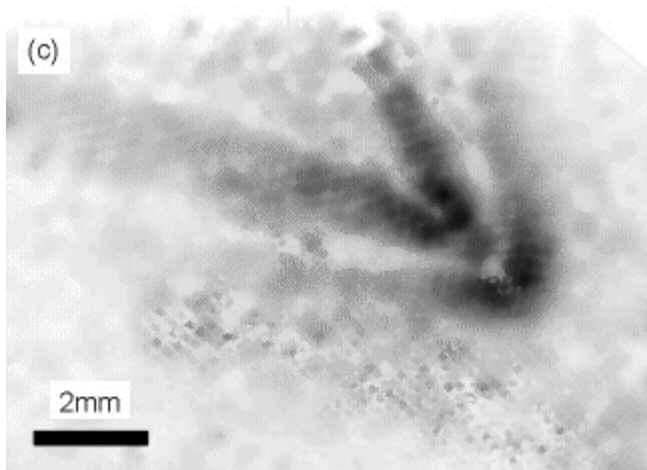


FIGURE 2. Map of particle speed in the lattice layer. Darker grays correspond to faster particles. A supersonic particle moving at 4 cm/sec moved toward the lower right, producing the Mach cones shown here.

Some peculiar features to note are the multiple cones and the rounded vertices. Analyzing the particle motion, we determined that the first cone is compressional, with particles displaced forward, while the second cone is rarefactive, with particles moving in the opposite direction. We attribute the presence of multiple cones to the strong coupling in the crystalline state. In our experiment, the particles were arranged in a crystalline lattice, and they were deformed elastically as the fast particle passed by. Unlike a gas atom, an atom in a crystal has a memory of its original position. When the crystal is deformed elastically, the atoms are restored toward this position. In our experiment, the particles over-shoot this equilibrium position, and oscillate about it. The oscillation is damped by the gas drag.

The rounded vertices are probably due to the finite size of the Debye sphere surrounding the fast particle. In gasdynamics, it is well known that a finite-size supersonic object, such as a sphere, creates a U-shaped Mach cone, in contrast to a needle-shaped object, which produces a V-shaped cone.

We carried out molecular dynamics simulations of these experiments. This was done using 2,500 particles, which we allowed to settle into equilibrium positions. We then injected an additional particle, which we constrained to move on a horizontal plane 200 microns below the lattice layer. These simulations also revealed multiple Mach cones. The simplicity of the physics in the simulation demonstrates the simple physical nature of the Mach cones.

As predicted by Havnes (16), Mach cones can be used as a diagnostic of the dusty plasma. In our case, we measured the particle charge, Q , from the Mach angle $\mu = \sin^{-1}(1/M)$, where $M = v/c$ is the Mach number of an object moving at speed v through a medium with an acoustic speed c . Doing this requires a model for the acoustic speed. In our case, with a strongly-coupled two-dimensional suspension and particles separated by a distance large compared to the Debye length, it is valid to use the DLW dispersion relation of Homan *et al.* (9). In the long-wavelength limit, $\lambda > 2\pi\Delta$, the DLW has only weak dispersion. Thus, the acoustic speed is a constant, as required for Mach cones. It happens to vary linearly with the particle charge Q . By measuring the Mach angle and the speed of the fast particle from the video, the particle separation from a correlation function analysis of a still image, and the Debye length from a Langmuir probe, we find a particle charge. In our case, Mach angle $\mu = 33.5^\circ \pm 3^\circ$ for the first second cone yields find $13,000 < -Q/e < 24,000$, where the uncertainty arises from the uncertainty in the Debye length. This result can be compared to our measurement using the resonance method, $-Q/e = 23,000$.

Further details of the Mach cone experiments and simulations will be reported elsewhere (18).

ACKNOWLEDGMENTS

The experiments reported here were carried out at MPE-Garching. Simulations and data analysis were carried out at Iowa. Funding for the Iowa group was from NSF and NASA.

REFERENCES

1. J. H. Chu and Lin I, *Phys. Rev. Lett.* **72**, 4009 (1994).
2. H. Thomas, G. Morfill, V. Demmel, J. Goree, B. Feuerbacher, and D. Möhlmann, *Phys. Rev. Lett.* **73**, 652 (1994).
3. Y. Hayashi and K. Tachibana, *Jpn. J. Appl. Phys.* **33**, 804 (1994).
4. A. Melzer, T. Trottenberg, and A. Piel, *Phys. Lett. A* **191**, 301 (1994).
5. T. Trottenberg, A. Melzer, and A. Piel, *Plasma Sources Sci. Technol.* **4**, 450 (1995).
6. O. Havnes, T. Aslaksen, T. W. Hartquist, F. Li, F. Melandsø, G. E. Morfill, and T. Nitter, *J. Geophys. Res.* **100**, 1731 (1995).
7. R. A. Quinn, C. Cui, J. Goree, J. B. Pieper, H. Thomas, and G. E. Morfill, *Phys. Rev. E* **53**, R2049 (1996).
8. J. B. Pieper and J. Goree, *Phys. Rev. Lett.* **77**, 3137 (1996).
9. A. Homann, A. Melzer, R. Madanio, and A. Piel, *Phys. Lett. A* **242**, 173 (1998).
10. U. Konopka, L. Ratke, and H. M. Thomas, *Phys. Rev. Lett.* **79**, 1269 (1997); and U. Konopka, unpublished.
11. S. Nunomura, N. Ohno, and S. Takamura, *Phys. Plasmas* **5**, 3517 (1998).
12. Y. K. Khodataev, S. A. Khrapak, A. P. Nefedov, and O. F. Petrov, *Phys. Rev. E* **57**, 7086 (1998).
13. D. A. Law, W.H. Steel, B. M. Annaratone, and J.E. Allen, *Phys. Rev. Lett.* **80**, 4189 (1998).
14. H. W. Liepman and A. Roshko, *Elements of Gas Dynamics* (Wiley, New York, 1957).
15. N. Cheng, Z. Zhu, C. H. Cheng and M. N. Toksöz, *Geophysical Prospecting* **42**, 303 (1994).
16. O. Havnes, T. Aslaksen, T. W. Hartquist, F. Li, F. Melandsø, G. E. Morfill, and T. Nitter, *J. Geophys. Res.* **100**, 1731 (1995).
17. F. Melandsø and J. Goree, Polarized Supersonic Plasma Flow Simulation for Charged Bodies such as Dust Particles and Spacecraft, *Phys. Rev. E* **52**, 5312-5326, (1995).
18. D. Samsonov, J. Goree, Z.W. Ma, A. Bhattacharjee, H.M. Thomas, and G.E. Morfill, submitted to *Phys. Rev. Lett.* (1999).